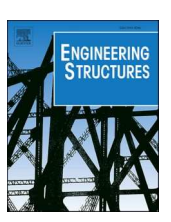
Contents lists available at ScienceDirect

Engineering Structures

journal homepage: www.elsevier.com/locate/engstruct





PI-LSTM: Physics-informed long short-term memory network for structural response modeling

Fangyu Liu^{a,d}, Junlin Li^{b,c,*}, Linbing Wang^{a,e,*}

- a Department of Civil and Environmental Engineering, Virginia Polytechnic Institute and State University, Blacksburg, VA, USA
- ^b Department of Structural Engineering, Tongji University, Shanghai 200092, China
- ^c State Key Laboratory of Disaster Reduction in Civil Engineering, Tongji University, Shanghai, China
- d Illinois Center for Transportation, Department of Civil and Environmental Engineering, University of Illinois Urbana-Champaign, Urbana, IL, USA
- e School of Environmental, Civil, Agricultural, and Mechanical Engineering, University of Georgia, Athens, GA, USA

ARTICLE INFO

Keywords: Deep learning Physics-informed long short-term memory network Structural response modeling Physics constraint

ABSTRACT

Deep learning models have achieved remarkable accuracy for structural response modeling. However, these models heavily depend on having a sufficient amount of training data, which can be challenging and time-consuming to collect. Moreover, data-driven models sometimes struggle to adhere to physics constraints. Therefore, in this study, a physics-informed long short-term memory (PI-LSTM) network was applied to structural response modeling by incorporating physics constraints into deep learning. The physics constraints were modified to accommodate the characteristics of both linear and nonlinear cases. The PI-LSTM network, inspired by and compared with existing physics-informed deep learning models (PhyCNN and PhyLSTM), was validated using the numerical simulation results of the single-degree-of-freedom (SDOF) system and the experimental results of the six-story building. Additionally, the PI-LSTM network underwent thorough investigation and validation across the four cases of the SDOF system and numerical simulation results of the six-story building with the comparison of the regular LSTM. The results indicate that the PI-LSTM network outperformed the regular LSTM models in terms of accuracy. Furthermore, the PI-LSTM network exhibited a more concentrated and higher accuracy range when analyzing the results of both the SDOF system and the six-story building. These findings demonstrate that the PI-LSTM network presents a reliable and efficient approach for structural response modeling.

1. Introduction

Infrastructures, encompassing buildings, pavements, bridges, and tunnels, play a crucial role in public life, directly impacting living standards and life safety. However, natural disasters, such as earth-quakes, pose significant challenges to infrastructure, often leading to reduced service life or even destruction. In light of this, ensuring the safe operation of infrastructure is of utmost importance. To address this, structural health monitoring has been developed to sense, detect, and evaluate the safety and health of infrastructure [1,2]. A key aspect of structural health monitoring is modeling the structural response accurately. Presently, there are two main approaches for structural response modeling: analytical methods and physics-based methods. Analytical methods involve employing various time series modeling techniques

such as autoregressive models [3], autoregressive moving average models [4], and autoregressive integrated moving average models [5]. Additionally, time history analysis based on the structural mechanics model has also been utilized for modeling structural response [6,7]. For instance, Lu et al. [6] developed an open-source workflow for urban building seismic damage simulation using time history analysis and multiple-degree-of-freedom models. However, these analytical methods still face challenges in terms of accuracy [8]. On the other hand, physics-based methods, particularly the finite element method (FEM), have gained popularity for modeling structural responses. FEM has been widely applied to simulate structural responses. For example, Zheng et al. [9] utilized FEM to simulate the small deformation in a three-story reinforced concrete frame, while they proposed a hybrid framework that combines FEM and physics engine to simulate the whole process of

E-mail addresses: lfangyu@illinois.edu (F. Liu), junlinli@tongji.edu.cn (J. Li), Linbing.Wang@uga.edu (L. Wang).

^{*} Corresponding authors at: Department of Structural Engineering, Tongji University, Shanghai 200092, China (J. Li). Department of Civil and Environmental Engineering, Virginia Polytechnic Institute and State University, Blacksburg, VA, USA (L. Wang).

building collapse. Wu et al. [10] applied FEM to investigate the seismic performance in a two-story, three-span Shanghai Metro station situated in soft soil and validated their finite element models with the experimental results. Meng and Lui [11] employed FEM to analyze the seimic responses of a skew reinforced concrete box girder bridge, studying the effects of external forces, boundary conditions, and structural parameters. While FEM offers high fidelity and accuracy, it is computationally expensive and sensitive to material properties, boundary conditions, and interaction between substructures. Consequently, efficiently and reliably modeling structural response, particularly under extreme loads, remains a significant challenge.

In recent times, the application of data-driven methods in structural response modeling has gained momentum due to the rapid development of technology. Deep learning, in particular, has emerged as a powerful and efficient tool for this purpose [1,12–17]. For example, Zhang et al. [12] proposed two schemes of the long-short term memory (LSTM) network to model and predict nonlinear structural responses, leveraging experimental data from a six-story instrumented building. Huang and Chen [13] employed the one-dimensional convolutional neural network (CNN) and LSTM network to model the seismic response of a two-story, three-span metro station, comparing their results with a baseline multilayer perceptron (MLP) model. Li et al. [14] developed an artificial neural network (ANN) framework for modeling the dynamic responses of the vehicle-bridge interaction system, incorporating a 3D train vehicle model, a bridge finite element model, and a wheel-rail contact model. Li et al. [1] proposed a new modeling paradigm utilizing 1D-CNN and the gated recurrent unit (GRU) for dam structural response modeling with validation conducted on a high arch dam using three monitoring items (dam displacement, crack opening displacement, and seepage). These studies have achieved exceptional accuracy; however, they heavily rely on the assumption of having sufficient data for training the deep learning models. Collecting a large amount of data is often time-consuming, expensive, and challenging, and purely data-driven models may not always adhere to physics constraints.

To address these challenges, integrating scientific knowledge into deep learning has emerged as a potential solution [8,18,19]. This approach aims to harness the benefits of both data-driven and knowledge-driven approaches. Various strategies have been employed to incorporate knowledge into deep learning models. For instance, the algebraic equation or logic rule has been included in the loss function to impose constraints during model training [20,21]. The knowledge graph has been introduced to provide information about relationships between instances [22], especially in the image classification task [23]. Furthermore, physical simulation has been utilized to augment and enrich training data [24].

Therefore, this work introduces a physics-informed long short-term memory (PI-LSTM) network for modeling structural responses. The main contributions of this work are summarized as follows:

- The physics-informed long short-term memory network was applied to modeling structural responses by incorporating physics constraints into deep learning. The physics constraints were modified to accommodate the characteristics of both linear and nonlinear cases.
- The PI-LSTM network, inspired by and compared with existing physics-informed deep learning models (PhyCNN and PhyLSTM), was validated using the numerical simulation results of the singledegree-of-freedom system and the experimental results from the six-story building.
- The performance of the PI-LSTM was further explored through four cases of the single-degree-of-freedom system subjected to ground motion and the numerical analysis of the six-story building under different earthquake ground motions. A comparison was made between the PI-LSTM network and the regular LSTM to assess the effectiveness of the PI-LSTM network.

2. Physics-informed long short-term memory (PI-LSTM)

Given that structural response data often takes the form of time series, modeling structural response can be considered a sequence prediction task. Extensive research has demonstrated that LSTM is a powerful and dependable tool for this type of task [25,26,27]. The strength of LSTM lies in its ability to capture long-term dependencies by selectively storing crucial information from the past and disregarding irrelevant or unimportant information [28,29]. However, traditional training strategies for deep learning models rely solely on data. Integrating scientific knowledge as the physics constraint during the training process could improve the robustness and reliability of the deep learning model [8]. Therefore, a physics-informed long short-term memory network is applied in this work for structural response modeling.

Let's revisit the fundamental equation (Eq. (1)) for structural dynamics based on the single-degree-of-freedom (SDOF) system.

$$m\ddot{x} + c\dot{x} + kx = F_E \tag{1}$$

where m, c, and k are the mass, damping coefficient, and stiffness; x, \dot{x} , and \ddot{x} are the displacement, velocity, and acceleration; F_E is the external force.

In the context of structural response modeling, ground motion is a commonly encountered scenario. When infrastructure is exposed to ground motion, the equation of motion for the SDOF system could be expressed as Eq. (2) or (3).

$$m\ddot{x} + c\dot{x} + kx = -m\ddot{x}_g \tag{2}$$

$$\ddot{x} + 2\xi\omega\dot{x} + \omega^2 x = -\ddot{x}_g, \ \omega = \sqrt{\frac{k}{m}} \text{ and } \xi = \frac{c}{2m\omega}$$
 (3)

where x, \dot{x} , and \ddot{x} are the relative displacement, velocity, and acceleration with respect to ground/support; \ddot{x}_g is the ground acceleration; ω is the structural frequency; ξ is the damping ratio.

The physics-informed long short-term memory network, as illustrated in Fig. 1, is applied to the structural response modeling under the ground motion. In structural response modeling, the input typically consists of the ground acceleration [8,13,30]. However, the current structural response is influenced not only by the current load but also by the previous structural response. Therefore, it is crucial to incorporate the previous structural response as an additional input. Therefore, in the PI-LSTM network, both the ground acceleration (\ddot{x}_g) and previous structural response (z) are considered as the input. The choice of the previous structural response (z) may vary depending on the specific design or measurement requirements. For instance, during shake table tests or field monitoring, the displacement and acceleration of buildings on the ground could be easily measured separately by the displacement sensor and accelerometer [31,32]. However, directly measuring displacement can sometimes be challenging. In such cases, researchers or engineers may derive displacement by integrating the measured acceleration to monitor the seismic response of underground structures [10,33]. Therefore, the previous structural response (2) could encompass both displacement and acceleration indicators or solely rely on one of these indicators. The output of the PI-LSTM network corresponds to the structural response, which shares the same indicators as the previous structural response. This will be further discussed in detail in Section 3.2. Once the input and output are defined, the LSTM network is constructed to establish the relationship between the input and output variables.

To incorporate scientific knowledge into the deep learning model, the equation of motion for the structural dynamics (i.e. scientific knowledge) is introduced as the physics constraint. This physics constraint involves the output structural response and the input ground acceleration. However, as indicated in Eq. (2) or (3), all three indicators (displacement, velocity, and acceleration) are required simultaneously,

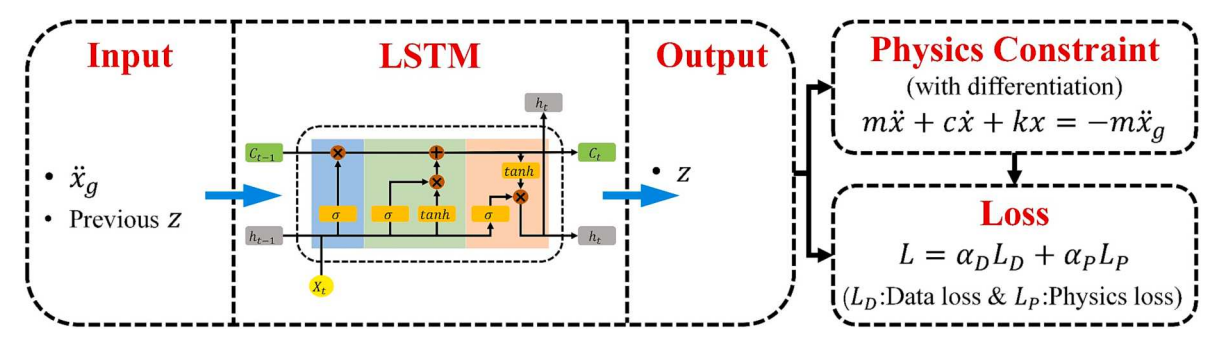


Fig. 1. Scheme of physics-informed long short-term memory (PI-LSTM) network. The input includes the ground acceleration (\ddot{x}_g) and the previous structural response (z). The output is the structural response (z). The total loss consists of the data loss from the difference between the prediction and ground truth and the physics loss from the physics constraint. Both α_D and α_P are set to 1 in this work.

which can pose challenges in experimental or field monitoring scenarios. To overcome this challenge, the differential method (e.g., the central finite difference method) is used to estimate the unknown indicators of the structural response. For instance, if the output structural response includes displacement and acceleration, the velocity could be obtained by taking the derivative of the predicted displacement. Subsequently, the output structural response (e.g., displacement and acceleration) and the structural response (e.g., velocity) obtained through the differential method are incorporated into the physics constraint alongside the input ground acceleration.

The total loss comprises two main components: data loss and physics loss. The data loss is calculated based on the disparity between the prediction and ground truth, a common metric used in LSTM models for time series prediction tasks. The physics loss is derived from the physics constraint, specifically the equation of motion for the structural dynamics. The physics loss could regularize the deep learning model, which helps to eliminate the overfitting issue, reduce the dependency on large training datasets, and enhance the robustness of the model. It is important to note that the loss function is solely utilized during the training process for deep learning models. The physics constraint, based on physics knowledge, is not applied during the validation or test phases. Both the data loss and physics loss utilize the mean square loss (i.e., MSELoss), a widely used metric in time series forecasting tasks.

Drawing upon the aforementioned concepts, the physics-informed long short-term memory network is constructed to model the structural response in the presence of ground motion. Nonetheless, this PILSTM network could be extended to address structural response modeling in various scenarios. It just needs to change the physics constraint and sometimes the target structural response.

3. SDOF numerical validation

The single-degree-of-freedom system serves as a quintessential and fundamental entity for comprehending and exploring structural dynamics. Consequently, the applicability and efficacy of the PI-LSTM network are initially assessed by employing it on the SDOF system subjected to ground motion. The data about ground motion is sourced from previous literature [8] and numerical analysis conducted via the finite element method. The architecture configuration of LSTM remains consistent throughout this section. According to PyTorch [34], LSTM comprised 4 recurrent layers and a hidden state with 100 features, while the dropout rate was 0.1. The optimization function was Adam [35], the training epoch was 500, and the learning rate was 0.001.

3.1. Comparison with the existing model

Zhang et al. [8] proposed a physics-guided convolutional neural network (PhyCNN) for modeling structural responses under ground motion and found their proposed PhyCNN demonstrated superior performance compared to the non-physics-guided neural network. Given

the model's effectiveness and the availability of data sources (datasets, model codes, and prediction results), PhyCNN was chosen for comparison with the PI-LSTM network to validate its reliability. Initially, the SDOF system results from their work were utilized to make a comparison with the PI-LSTM network. They employed 100 independent seismic sequences from the PEER strong-motion database [36] as the input to the SDOF system, generating simulation results of 50 s each at a frequency of 20 Hz, resulting in 1001 data points per simulation. Since they made their data, codes, and results publicly available, a fair comparison was facilitated by replacing their PhyCNN model with the PI-LSTM network. In their study, 10 samples were selected from the total 100 samples as training data, while the remaining 90 samples were treated as test data to evaluate model performance. This procedure was also followed in training and evaluating the PI-LSTM network in the present work

Table 1 provides a summary of the comparison between PhyCNN and PI-LSTM. In Zhang et al.'s work, the input was the ground acceleration, while the output comprised displacement, velocity, and restoring force. To incorporate physical constraints, they incorporated the equation of motion and also considered the discrepancy between the predicted velocity and the derivative of the predicted displacement as part of the physical loss. Fig. 2 and Table 2 illustrate the performance of PhyCNN and PI-LSTM in predicting displacement, acceleration, and restoring force. Overall, PI-LSTM exhibited significantly higher accuracy than PhyCNN across all three indicators. The accuracy of PhyCNN displayed more variability over a wider range, with the mean accuracy for all three indicators being lower than the median accuracy when evaluated on the test data (consisting of 90 samples). Conversely, the accuracy of PI-LSTM was concentrated within a narrower range, with the mean and median accuracy being much closer for all three indicators.

In addition to PhyCNN, Zhang et al. [30] also developed physics-informed multi-LSTM networks for structural metamodeling of nonlinear structures. Their models were able to integrate physics

Table 1Summary of the comparison between PhyCNN and PI-LSTM.

	PhyCNN	PI-LSTM
Input	$\ddot{x_g}$	\ddot{x}_g & Previous $\{x, \dot{x}, F_{rs}\}$
Output	x,\dot{x},F_{rs}	x, \dot{x}, F_{rs}
Data Loss (L_D)	$\frac{1}{N}\Big(\ x^p-x^m\ _2^2+$	$-\ \dot{\pmb{x}}^p-\dot{\pmb{x}}^m\ _2^2+\ F_{rs}^p-F_{rs}^m\ _2^2\Big)$
Physics Loss (L_P)	$rac{1}{N}\Big(\ \dot{\mathbf{x}}^p-\dot{\mathbf{x}}_t^p\ _2^2+$	$\left\ \ddot{\mathbf{x}}_{t}^{p}+F_{rs}^{p}+\ddot{\mathbf{x}}_{g}\right\ _{2}^{2}$
Total Loss (L)	$L = L_D + L_P$	

Note: (1) F_{rs} is the mass-normalized restoring force, (2) the superscript p and m denote the prediction and ground truth, respectively, (3) the subscript t denotes the derivative of the prediction. E.g. $\dot{x}_t^p = \frac{dx^p}{dt}$, and $(4)\|u\|_2^2 = \left(\sqrt{\sum_i x_i^2}\right)^2 = \sum_i x_i^2$.

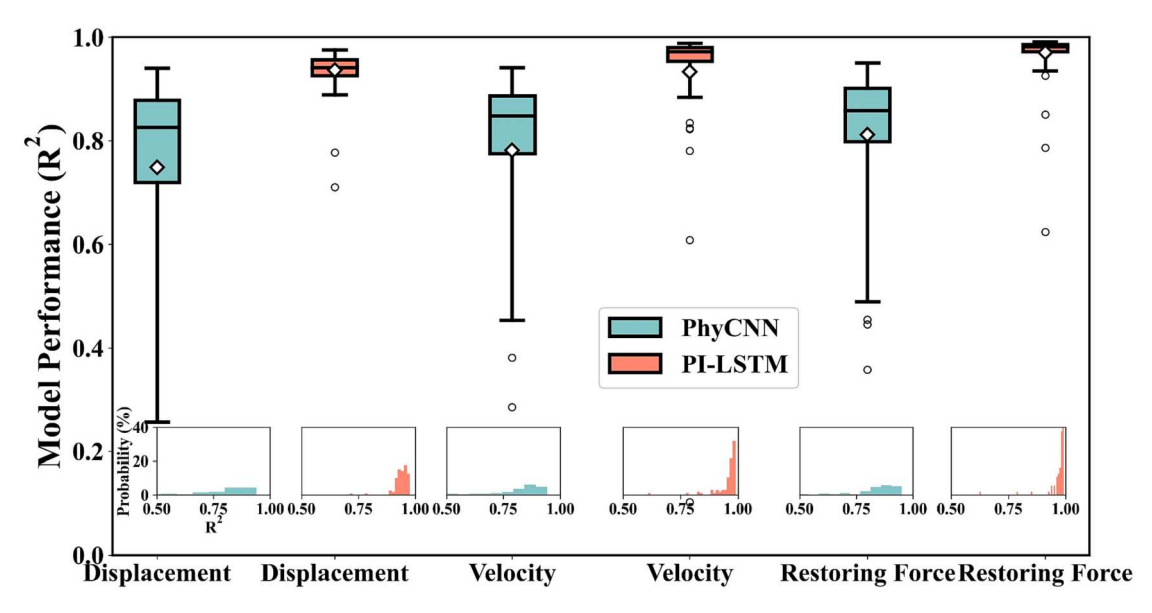


Fig. 2. Performance of PhyCNN and PI-LSTM for predicting displacement, velocity, and restoring force.

Table 2
Summary of model performance of PhyCNN, PhyLSTM, and PI-LSTM.

Metric	Metric PhyCNN		PhyLSTM	PhyLSTM		PI-LSTM			
	Dis.	Vel.	RF	Dis.	Vel.	RF	Dis.	Vel.	RF
\mathbb{R}^2	0.75 ± 0.25	0.78 ± 0.23	0.81 ± 0.15	0.94 ± 0.09	0.92 ± 0.11	$\textbf{0.75} \pm \textbf{0.19}$	0.94 ± 0.04	0.93 ± 0.15	0.97 ± 0.05
RMSE	0.02 ± 0.02	0.12 ± 0.10	0.58 ± 0.61	0.01 ± 0.01	0.08 ± 0.07	0.63 ± 0.37	0.01 ± 0.004	0.05 ± 0.02	0.18 ± 0.13
MAE	0.01 ± 0.01	0.07 ± 0.06	0.32 ± 0.35	0.01 ± 0.01	0.04 ± 0.03	0.32 ± 0.20	0.01 ± 0.003	0.03 ± 0.01	0.10 ± 0.06

Note: Dis. is displacement, Vel. is velocity, and RF is restoring force. RMSE is the root mean squared error and MAE is the mean absolute error. The results shown in this table are the mean value + the standard deviation.

knowledge to improve the learning of sequence-to-sequence features. To provide a comprehensive comparison, these models were also included in the analysis. As shown in Table 2, PI-LSTM and PhyLSTM demonstrated similar accuracy in predicting displacement and velocity. However, PI-LSTM outperformed PhyLSTM in predicting restoring force. In the case of PI-LSTM and PhyCNN, the accuracy of restoring force surpassed that of both displacement and velocity. Conversely, for PhyLSTM, the accuracy of restoring force was lower compared to the other two structural responses. This difference can be attributed to the fact that PI-LSTM and PhyCNN directly predict all structural responses (displacement, velocity, and restoring force), whereas PhyLSTM predicts the restoring force based on the displacement and velocity predicted in the previous step. This distinction leads to varied performance across the three structural responses among these three models. The comparison between these three models (PI-LSTM, PhyCNN, and PhyLSTM) provides strong validation for the effectiveness and reliability of the PI-LSTM network.

3.2. Case study

One limitation of Zhang et al.'s work [8] was that their SDOF system was primarily approached from a mathematical standpoint rather than being anchored in engineering applications. This raises concerns about the reliability of their numerical findings, as their SDOF system employed a mass of 1 kg, a damping coefficient of 1 Ns/m, and a linear stiffness of 20 N/m. To address this issue, the SDOF system with parameters resembling those of a one-story concrete building was utilized to build the dataset. The same earthquake records as Zhang et al.'s work [8] were adopted for consistency. In the SDOF system, the mass was set to 100 tons, corresponding to a period of 0.5 s (i.e., the stiffness is 15791367 N/m), and a damping ratio of 0.05 (i.e., the damping

coefficient is 125664 Ns/m). The numerical analysis of the SDOF system under ground motion was conducted using OpenSees [37]. Fig. 3 illustrates a sample of the ground acceleration, structural displacement, structural velocity, and structural acceleration in the SDOF system. Following the same data preprocessing procedures employed by Zhang et al. [8], 10 samples were selected from all 100 samples as the training data, while the remaining 90 samples were designated for testing the model's performance. The satisfactory convergence of models also supports the adequacy of solely employing the training data and test data, as will be discussed in the subsequent section.

To evaluate the effectiveness of the PI-LSTM network, various cases will be examined using various outputs. It should be noted that both the training and test earthquake records remained consistent across all cases. To establish a basis for comparison, the regular LSTM without the physics loss, denoted as "LSTM", is employed to compare with the PI-LSTM network in this section.

3.2.1. Case 1: Predicting x, \ddot{x}

Displacement and acceleration are widely recognized as essential indicators for monitoring purposes during shake table tests or field monitoring [31,32]. As a result, both displacement and acceleration are regarded as the output structural response. Table 3 provides an overview of the key differences between LSTM and PI-LSTM. The input of PI-LSTM consisted of the ground acceleration and previous structural responses (i.e., displacement and acceleration), while the output of PI-LSTM was displacement and acceleration. The total loss of PI-LSTM comprised both the data loss and physics loss, whereas the total loss of LSTM only accounted for the data loss. Fig. 5a and Table 4 summarize the results of LSTM and PI-LSTM for predicting displacement and acceleration. Overall, PI-LSTM demonstrated higher accuracy compared to LSTM. Furthermore, when examining the accuracy distribution of the test data,

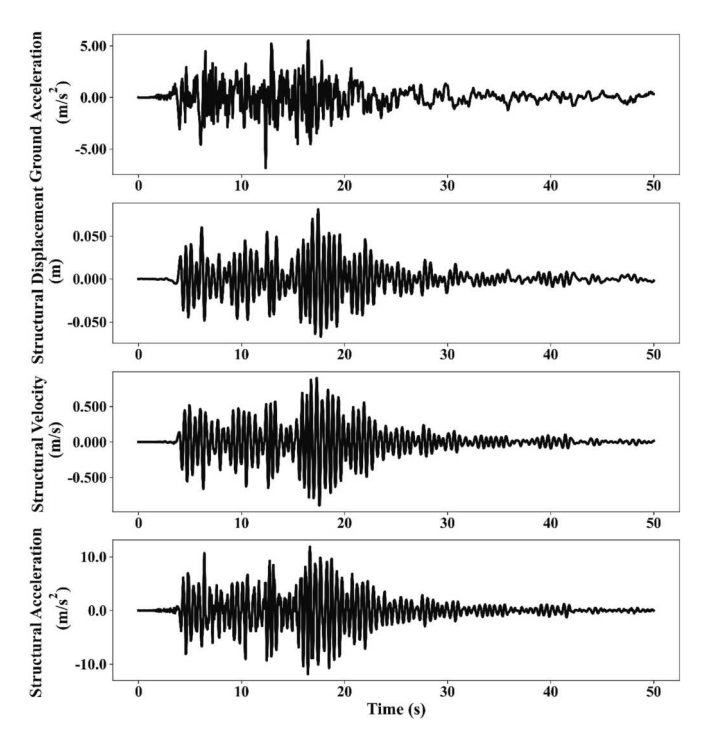


Fig. 3. Data for the ground acceleration, structural displacement, structural velocity, and structural acceleration.

PI-LSTM exhibited greater robustness and stability than LSTM, as the accuracy values of PI-LSTM were concentrated within a narrower range.

Furthermore, one notable advantage of physics-informed deep learning models lies in their ability to achieve remarkable performance even with limited training data, owing to the incorporation of prior physics knowledge. However, a pertinent question arises: Will physicsinformed deep learning models continue to outperform traditional deep learning models when provided with relatively abundant training data? To investigate this notion, a larger quantity of training data would be utilized for model training. The case involving 10 training samples could serve as a baseline, while additional sets of 20, 30, 40, 50, and 60 training samples would be used to train both LSTM and PI-LSTM. Fig. 6 illustrates the performance of LSTM and PI-LSTM across different numbers of training samples. As depicted in Fig. 5a and Fig. 6, when confronted with a limited quantity of training data (10 samples), PI-LSTM surpassed LSTM significantly. Nevertheless, as the number of training samples increased from 10 to 60, both LSTM and PI-LSTM exhibited enhanced accuracy, with LSTM experiencing a particularly

noteworthy improvement. The gap between LSTM and PI-LSTM decreased substantially, and these two models demonstrated highly similar performance after the number of training samples reached 40. Although LSTM displayed slightly lower accuracy in displacement compared to PI-LSTM, both models exhibited similar accuracy in acceleration. This implies that physics-informed deep learning models could outperform traditional deep learning models when confronted with limited training data. However, once a sufficient amount of training data is obtained, traditional and physics-informed deep learning models tend to exhibit comparable performance.

3.2.2. Case 2: Predicting x

Displacement serves as a valuable indicator of the structural condition and a descriptor of structural deformation behavior. When monitoring the structural condition of a building on the ground, it becomes essential to measure displacement as it provides crucial information while mitigating the impact of accelerometer noise. Therefore, the case of predicting displacement exclusively is applied to investigate the performance of the PI-LSTM network. Table 3 provides a summary of the comparison between LSTM and PI-LSTM regarding displacement prediction. The input of PI-LSTM consisted of the ground acceleration and previous structural responses (i.e., displacement), while the output was solely the displacement. In terms of the physics loss, both velocity and acceleration were derived from the displacement. Fig. 5b and Table 4 present the results of LSTM and PI-LSTM for predicting displacement. The predicted acceleration was obtained by taking the second-order derivative of the predicted displacement. This predicted acceleration was then used to assess the accuracy of the deep learning model by comparing it with the ground truth (acceleration obtained from the numerical results). Notably, PI-LSTM achieved higher accuracy in predicting displacement and demonstrated greater robustness and stability compared to LSTM. Furthermore, even after calculating acceleration from the predicted displacement, the predicted acceleration of PI-LSTM remained closer to the ground truth compared to LSTM.

3.2.3. Case 3: Predicting \ddot{x}

Acceleration is a widely used metric in structural health monitoring due to its relative ease of measurement. In certain monitoring scenarios, researchers or engineers may only have access to acceleration data during shake table tests or field monitoring [10,33]. Hence, it is crucial to assess the performance of deep learning models specifically designed to predict acceleration. When only an accelerometer is installed on a structure, double integration of the acceleration is typically required to obtain displacement. However, there are inherent challenges associated with double integration, such as defining initial or boundary conditions and dealing with noise [8,38]. Consequently, concerns arise regarding the accuracy of displacement prediction based on predicted

Table 3Summary of the comparison between LSTM and PI-LSTM.

	Case 1		Case 2		Case 3		Case 4	
	LSTM	PI-LSTM	LSTM	PI-LSTM	LSTM	PI-LSTM	LSTM	PI-LSTM
Input	ÿ _g & Pre	evious $\{x, \ddot{x}\}$	ÿ _g & Pr∈	evious {x}	ÿ _g & Pr∈	evious {x}	ÿ _g & Pr∈	evious $\{x, F_{rs}\}$
Output	x,\ddot{x}		x		x		x, F_{rs}	
Data Loss (L_D)	$\frac{1}{N}\Big(\ x^p$	$-x^{m}\ _{2}^{2}+\ \ddot{x}^{p}-\ddot{x}^{m}\ _{2}^{2}\Big)$	$\frac{1}{N}\Big(\ x^p\ $	$-x^{n}\Vert_{2}^{2}\Big)$	$\frac{1}{N} \bigg(\ \ddot{x}_t^p \bigg)$	$-\ddot{\mathbf{x}}^{n}\Vert_{2}^{2}$	$\frac{1}{N} \left(\ \ddot{x}_t^p \right.$	$-\ddot{x}^{m}\ _{2}^{2}+\ F_{rs}^{p}-F_{rs}^{m}\ _{2}^{2}$
Physics Loss (L _P)	-	$\frac{1}{N} \bigg(\left\ \ddot{\mathbf{x}}^p + 2\xi \omega \dot{\mathbf{x}}_t^p + \omega^2 \mathbf{x}^p + \ddot{\mathbf{x}}_g \right\ _2^2 \bigg)$	-	$\frac{1}{N} \left(\left\ \ddot{\mathbf{x}}_t^p + 2\xi \omega \dot{\mathbf{x}}_t^p + \omega^2 \mathbf{x}^p + \ddot{\mathbf{x}}_g \right\ _2^2 \right)$	-	$\frac{1}{N} \left(\left\ \ddot{\boldsymbol{x}}_t^p + 2\xi \omega \dot{\boldsymbol{x}}_t^p + \omega^2 \boldsymbol{x}^p + \ddot{\boldsymbol{x}}_g \right\ _2^2 \right)$	-	$\frac{1}{N} \left(\left\ \ddot{\mathbf{x}}_t^p + F_{rs}^p + \ddot{\mathbf{x}}_g \right\ _2^2 \right)$
Total	L =	$L = L_D + L_P$	L =	$L = L_D + L_P$	L =	$L = L_D + L_P$	L =	$L = L_D + L_P$
Loss (L)	L_D		L_D		L_D		L_D	

Note: (1) F_{rs} is the mass-normalized restoring force, (2) the superscript p and m denote the prediction and ground truth, respectively, (3) the subscript t denotes the derivative of the prediction. E.g. $\dot{x}_t^p = \frac{dx^p}{dt}$, and $(4)\|u\|_2^2 = \left(\sqrt{\sum_i x_i^2}\right)^2 = \sum_i x_i^2$.

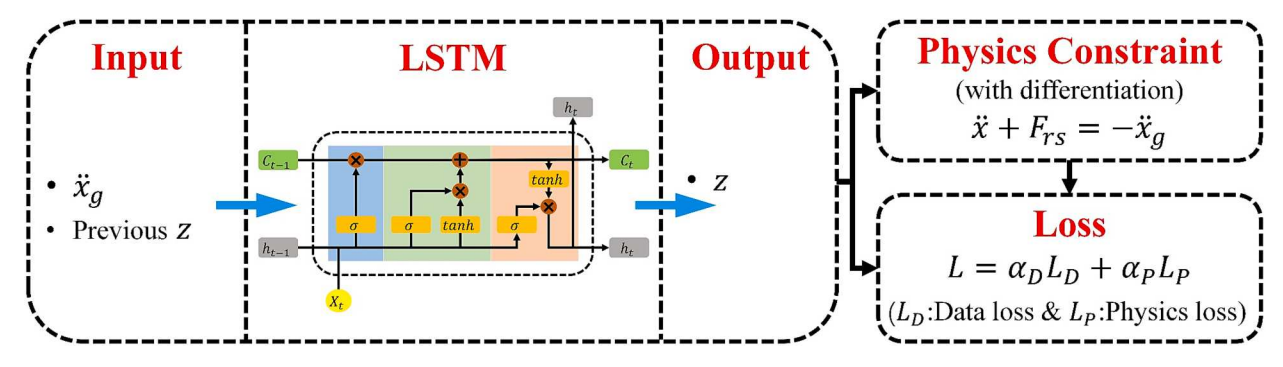


Fig. 4. Scheme of the PI-LSTM network for nonlinear analysis.

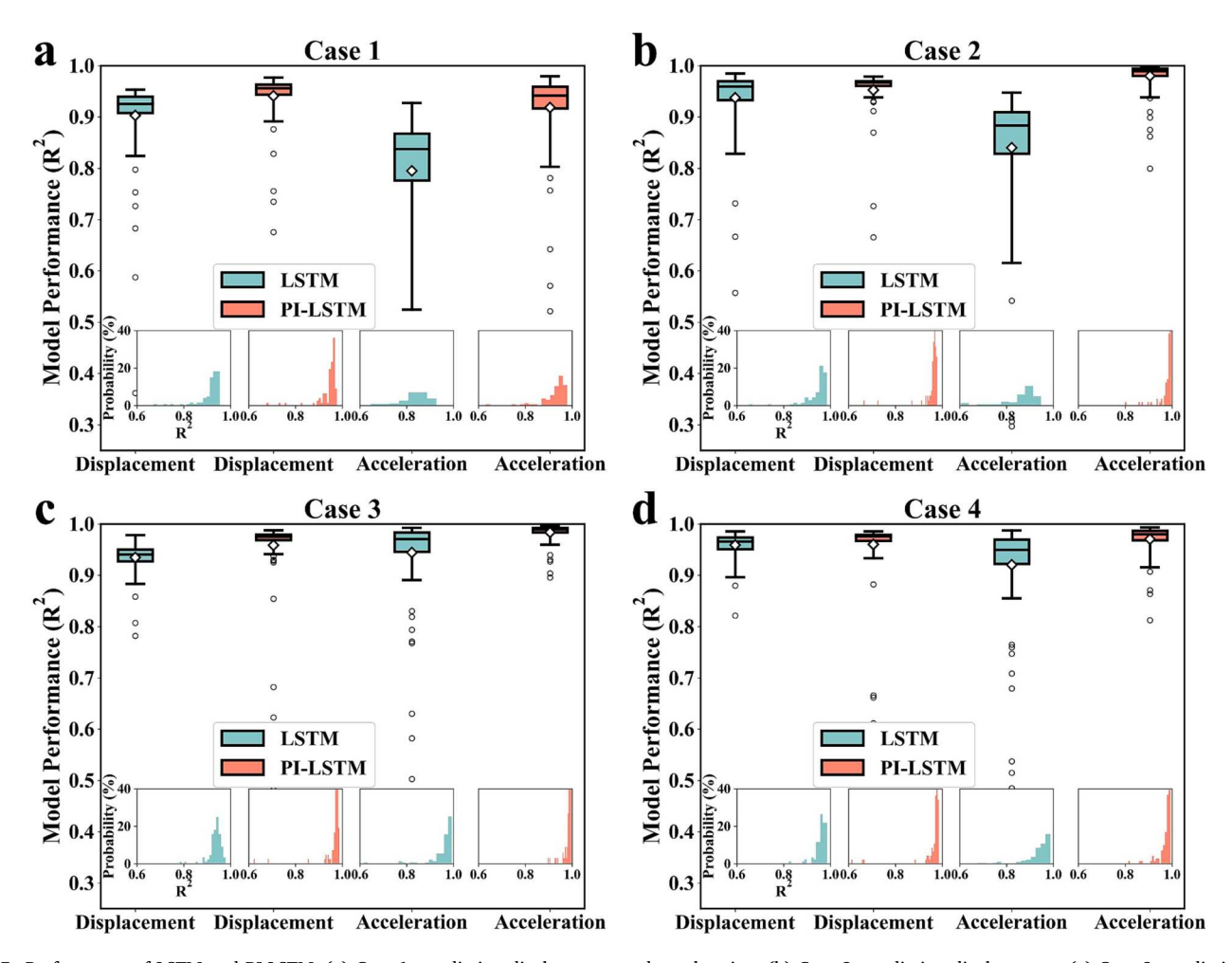


Fig. 5. Performance of LSTM and PI-LSTM. (a) Case 1: predicting displacement and acceleration, (b) Case 2: predicting displacement, (c) Case 3: predicting acceleration, and (d) Case 4: predicting acceleration (nonlinear analysis).

acceleration. To address this, displacement is considered as the output of the deep learning model, while the predicted acceleration is obtained from the second-order derivative of the predicted displacement. This predicted acceleration is then compared with the ground truth, which refers to the acceleration obtained from numerical results, to train the deep learning model. Table 3 provides a summary of the comparison between LSTM and PI-LSTM in terms of predicting acceleration. As previously mentioned, the input of PI-LSTM consisted of ground acceleration and previous structural responses (i.e., displacement), while the output of PI-LSTM was displacement. The data loss was calculated based on the difference between the predicted acceleration (i.e., the second-order derivative of the model output) and the ground truth (i.e., the

acceleration derived from the numerical results). The physics loss involved obtaining both acceleration and velocity by taking derivatives of the model output. Fig. 5c and Table 4 summarize the performance of LSTM and PI-LSTM in predicting acceleration. PI-LSTM consistently achieved higher and more stable accuracy compared to LSTM. The accuracy distribution of the test data demonstrates that PI-LSTM outperformed LSTM in terms of accuracy and robustness.

3.2.4. Case 4: Predicting \ddot{x} (nonlinear analysis)

When analyzing the motion of structures in nonlinear scenarios, it becomes challenging to rely on constant parameters, such as stiffness, to accurately describe their deformations. Consequently, applying the Case 3

Table 4Summary of the performance of LSTM and PI-LSTM.

Case 1					
Metric	LS	ТМ	PI-L	STM	
	Displacement	Acceleration	Displacement	Acceleration	
R^2	0.903 ± 0.082	0.795 ± 0.138	0.941 ± 0.048	0.918 ± 0.077	
RMSE	0.005 ± 0.002	1.232 ± 0.405	0.004 ± 0.001	0.756 ± 0.320	
MAE	0.003 ± 0.001	0.618 ± 0.284	0.002 ± 0.001	0.340 ± 0.178	
Case 2					

Metric	LSTM		PI-L	STM	
	Displacement	Acceleration	Displacement	Acceleration	
R^2	0.937 ± 0.063	0.840 ± 0.125	0.953 ± 0.061	0.980 ± 0.031	
RMSE	0.004 ± 0.001	1.057 ± 0.350	0.003 ± 0.001	0.334 ± 0.204	
MAE	0.002 ± 0.0004	0.537 ± 0.244	0.002 ± 0.001	0.173 ± 0.126	

Metric	LSTM		PI-LSTM	
	Displacement	Acceleration	Displacement	Acceleration
R^2	0.935 ± 0.030	0.944 ± 0.083	0.958 ± 0.071	0.984 ± 0.018
RMSE	0.004 ± 0.001	0.552 ± 0.325	0.003 ± 0.001	0.334 ± 0.157
MAE	0.002 ± 0.001	0.280 ± 0.204	0.002 ± 0.001	0.179 ± 0.101

	Case 4						
Metric	LS	гм	PI-LSTM				
	Displacement	Acceleration	Displacement	Acceleration			
R^2	0.959 ± 0.024	0.920 ± 0.095	0.960 ± 0.060	0.970 ± 0.030			
RMSE	0.003 ± 0.001	0.702 ± 0.345	0.003 ± 0.001	0.465 ± 0.253			
MAE	0.002 ± 0.001	0.359 ± 0.224	0.002 ± 0.001	0.200 ± 0.117			

Note: RMSE is the root mean squared error and MAE is the mean absolute error. The results shown in this table are the mean value \pm the standard deviation.

equation of motion (Eq. (2) or (3)) as the physics constraint in the PI-LSTM network becomes difficult. To overcome this issue, one potential solution is to combine the stiffness force and damping force to form the restoring force. Consequently, the equation of motion (Eq. (2) or (3)) could be re-written as follows:

$$\ddot{x} + F_{rs} = -\ddot{x}_g \tag{4}$$

where F_{rs} is the mass-normalized restoring force.

This equation (Eq.(4)) would serve as the physics constraint for the PI-LSTM network. Fig. 4 illustrates the architecture of the PI-LSTM network designed for nonlinear analysis. In comparison to the original PI-LSTM architecture (shown in Fig. 1), this modified model preserves

the LSTM architecture while altering the physics constraint and the corresponding structural responses (z) to accommodate nonlinear analysis requirements. To evaluate the performance of this modified PILSTM network, a specific case is selected for comparison with LSTM. As previously mentioned, acceleration is a commonly monitored indicator of structural condition. Therefore, PI-LSTM and LSTM were compared in terms of predicting acceleration. The dataset utilized was the same as in the other cases, but the mass-normalized restoring force (F_{rs}) was derived from the ground acceleration and structural acceleration, specifically $F_{rs} = -\ddot{x}_g - \ddot{x}$, to construct the dataset.

Table 3 provides a comprehensive comparison between LSTM and PI-LSTM in terms of predicting acceleration in the context of nonlinear analysis. Both LSTM and PI-LSTM utilized the ground acceleration and previous structural responses (displacement and mass-normalized restoring force) as inputs, while the outputs consisted of displacement and mass-normalized restoring force for both models. In Case 3, as described in Section 3.2.3, the displacement was considered the model output for predicting acceleration, resulting in reduced errors. The data loss was calculated by measuring the difference between the model's predictions (acceleration and mass-normalized restoring force) and the corresponding ground truth values obtained from the numerical results. Additionally, the physics loss was computed based on the physics constraint imposed by the modified equation (Eq.(4)). Fig. 5d and Table 4 present the results of LSTM and PI-LSTM for predicting acceleration in the context of nonlinear analysis. PI-LSTM consistently outperformed LSTM in terms of accuracy. Moreover, the accuracy distribution of the test data for PI-LSTM demonstrated a more concentrated range compared to that of LSTM, indicating its superior performance in predicting both displacement and acceleration.

4. Experimental and numerical validation

To further validate the performance of the PI-LSTM network, it is essential to assess its effectiveness using experimental or numerical results. However, due to the limited availability of publicly accessible benchmark experimental data, numerical analysis based on the finite element method serves as a suitable alternative. The process involves constructing a finite element model that aligns with the experimental conditions, including building parameters and boundary conditions. Subsequently, the structural response of the finite element model is computed under the experimental loading conditions. If the simulation results closely resemble the experimental findings, it instills confidence in using the finite element model to explore different scenarios, such as diverse ground motions. In this study, both experimental and numerical

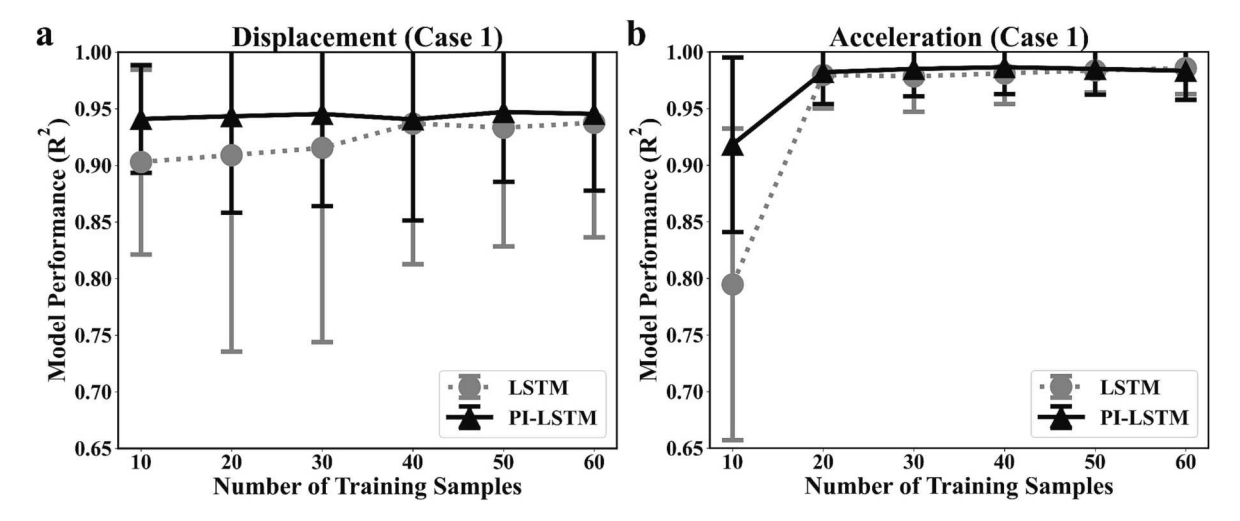


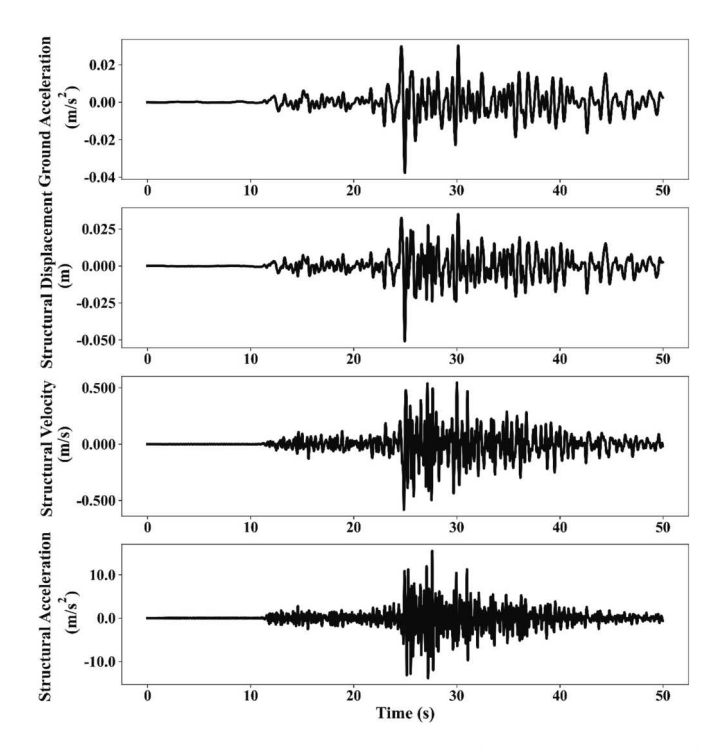
Fig. 6. Performance of LSTM and PI-LSTM with different numbers of training samples for Case 1. (a) Displacement and (b) acceleration. The results are the mean value and the standard deviation.

results were employed to evaluate the performance of the PI-LSTM network for a multi-story building subjected to ground motion. The LSTM architecture utilized in this section mirrors the architecture described in Section 3. As per the PyTorch library [34], the LSTM comprised 4 recurrent layers and 500 features in the hidden state, with a dropout rate of 0.1. The Adam optimization function [35] was employed, with a training epoch of 3000 and a learning rate of 0.001.

4.1. Experimental validation

Zhang et al. [8] utilized the experimental results from a 6-story hotel building located in San Bernardino, California, to investigate the performance of their proposed PhyCNN model. This building, designed in 1970 was equipped with nine accelerometers positioned on the first and third floors, as well as the roof. Twenty-one available records were obtained from the Center for Engineering Strong Motion Data (CESMD) [39] to build the dataset. Further detailed information regarding this dataset could be found in the previous literature [8]. Fig. 7 illustrates a sample from the dataset, depicting the ground acceleration, structural displacement, structural velocity, and structural acceleration. Eleven samples were designated as the training data, four samples were chosen for evaluation purposes, and the remaining six samples were allocated as test data for model assessment.

The deep learning model used in this study aimed to predict acceleration based on the data collected from installed accelerometers on the building. However, the process of obtaining displacement from acceleration through double integration could introduce errors, as mentioned earlier. To address this issue, a similar approach to Section 3.2.4 was employed, where the output of the deep learning model was treated as displacement, and the predicted acceleration was obtained by taking the second-order derivative of the predicted displacement. It is important to note that unlike the cases described in Section 3.2.4, the authors of Zhang et al. [8] did not incorporate the equation of motion as a physics constraint in their PhyCNN model. In their proposed PhyCNN model, displacement was the output, and the predicted acceleration was obtained by taking the second-order derivative of the predicted displacement. The loss function for this model was solely based on the difference



 $\textbf{Fig. 7.} \ \ \textbf{Data for the ground acceleration, structural displacement, structural velocity, and structural acceleration.}$

between the predicted acceleration and the ground truth. In this work, the PI-LSTM network was utilized for nonlinear analysis of the structural response, as discussed in Section 3.2.4. The experimental results presented in this study fall under the category of nonlinear analysis of structural response, making the PI-LSTM network (depicted in Fig. 4) suitable for modeling the structural response based on these experimental findings. Table 5 provides a summary of the comparison between PhyCNN and PI-LSTM in terms of predicting acceleration, specifically focusing on modeling the experimental results. The input for PI-LSTM consisted of the ground acceleration and previous structural responses (displacement and mass-normalized restoring force), while the input for PhyCNN only included the ground acceleration. The output of PI-LSTM was displacement and mass-normalized restoring force, whereas PhyCNN solely produced displacement as its output. The loss function for PI-LSTM encompassed two components: the data loss, calculated from the difference between the predicted and ground truth values, and the physics loss, derived from the physics constraint. In contrast, the loss function for PhyCNN was determined solely by the disparity between the predicted acceleration and the experimental results.

Fig. 8 and Table 6 present the performance comparison between PhyCNN and PI-LSTM in terms of predicting acceleration specifically for the third floor and roof. Additionally, Fig. 9 displays the corresponding predicted displacement and acceleration for both the third floor and the roof. Regarding the third floor, both PI-LSTM and PhyCNN exhibited similar accuracy in predicting displacement. However, when it came to predicting acceleration, PI-LSTM outperformed PhyCNN significantly in terms of accuracy. For the roof, PI-LSTM achieved higher accuracy than PhyCNN in predicting both displacement and acceleration. In particular, PI-LSTM displayed notably superior accuracy compared to PhyCNN in predicting acceleration. Its higher accuracy positions PI-LSTM as a more reliable option based on the results of this experiment.

Based on Fig. 9, the structural response, including displacement and acceleration, of the roof was higher compared to that of the third floor. When focusing on the displacement of the third floor (Fig. 8a), PhyCNN and PI-LSTM exhibited similar performance. However, as the monitoring location shifted to the roof, and the displacement increased, PI-LSTM outperformed PhyCNN in predicting the displacement of the roof (Fig. 8b). The superiority of PI-LSTM became even more pronounced when considering acceleration as the monitoring indicator. PI-LSTM demonstrated significantly higher accuracy than PhyCNN in predicting the acceleration of the third floor (Fig. 8a), although PhyCNN still achieved a satisfactory accuracy level with an R² value of 0.86. However, when the monitoring location shifted to the roof, the acceleration accuracy of PhyCNN dropped to 0.71, while PI-LSTM maintained a high level of accuracy, even surpassing that of the third floor (Fig. 8b). The disparity in acceleration accuracy between PI-LSTM and PhyCNN further widened as the amplitude and range of the acceleration increased. Additionally, both for displacement and acceleration, the accuracy distribution of PI-LSTM was concentrated within a smaller range compared to PhyCNN. In conclusion, it can be stated that PI-LSTM offers a more accurate and robust approach to structural response modeling. Particularly when dealing with higher amplitudes and wider ranges of the monitoring indicator, the advantages of PI-LSTM become even more prominent.

Table 5Summary of the comparison between PhyCNN and PI-LSTM.

	PhyCNN	PI-LSTM
Input	$\ddot{x}_{ m g}$	\ddot{x}_g & Previous $\{x, F_{rs}\}$
Output	x	x, F_{rs}
Data Loss (L_D)	$\frac{1}{N}\bigg(\ \ddot{\mathbf{x}}_t^p - \ddot{\mathbf{x}}^m\ _2^2\bigg)$	$rac{1}{N}igg(\ \ddot{\mathcal{X}}_t^p - \ddot{\mathcal{X}}^m \ _2^2 + \ F_{rs}^p - F_{rs}^m \ _2^2 igg)$
Physics Loss (L_P)	-	$rac{1}{N}igg(\left\ \ddot{\mathbf{x}}_t^p+F_{rs}^p+\ddot{\mathbf{x}}_g ight\ _2^2igg)$
Total Loss (L)	$L = L_D$	$L = L_D + L_P$

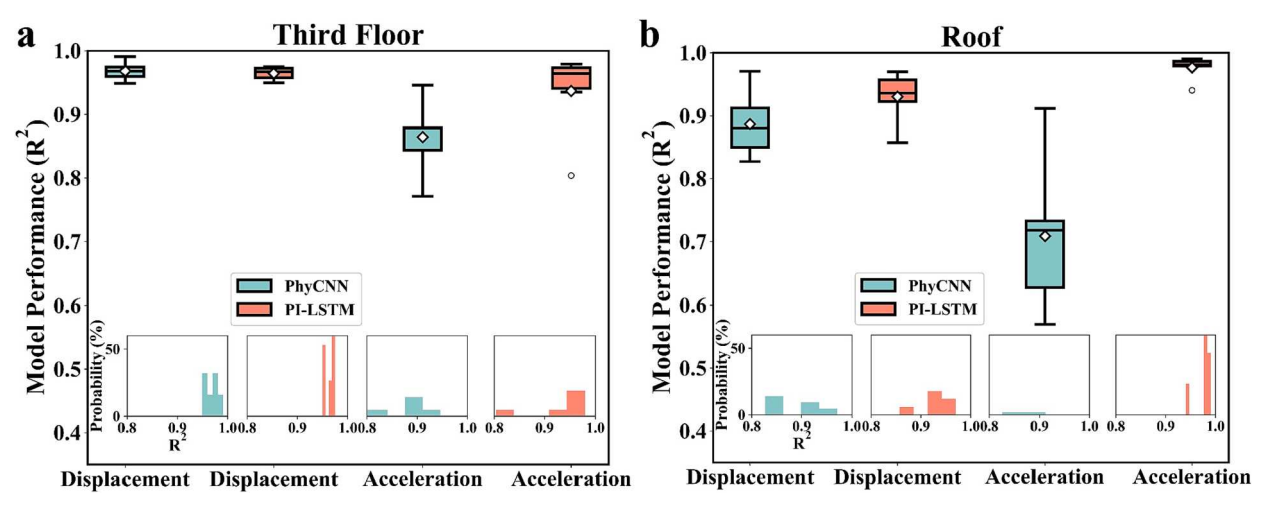


Fig. 8. Performance of PhyCNN and PI-LSTM for predicting the structural response in terms of the (a) third floor and (b) roof.

Table 6Summary of model performance of PhyCNN and PI-LSTM.

Third Floor						
Metric	PhyCNN		PI-LSTM			
	Displacement	Acceleration	Displacement	Acceleration		
R ²	0.968 ± 0.013	0.864 ± 0.053	0.965 ± 0.009	0.937 ± 0.061		
RMSE	0.001 ± 0.001	0.364 ± 0.161	0.001 ± 0.001	0.210 ± 0.062		
MAE	0.001 ± 0.0003	0.181 ± 0.099	0.001 ± 0.001	0.096 ± 0.035		
Roof						
Metric	PhyCNN		PI-LSTM			
	Displacement	Acceleration	Displacement	Acceleration		
R ²	0.887 ± 0.048	0.709 ± 0.111	0.930 ± 0.037	0.977 ± 0.017		

Note: RMSE is the root mean squared error and MAE is the mean absolute error. The results shown in this table are the mean value \pm the standard deviation.

 0.002 ± 0.002

 0.001 ± 0.001

 0.280 ± 0.088

 0.145 ± 0.054

 1.094 ± 0.515

 0.550 ± 0.312

4.2. Numerical validation

 0.002 ± 0.001

 0.001 ± 0.001

RMSE

MAE

In addition to the experimental results, the numerical simulation of a six-story building was conducted to evaluate the performance of the PI-

LSTM model. This six-story building, as described in previous literature [40], was designed in 1976 based on the 1973 UBC requirements [41]. Information regarding this building was selected from the California Strong Motion Instrumentation Program (CSMIP). The building had dimensions of 36.60 m by 36.60 m in plan, with six bays in one direction $(6\times6.10$ m). The elevation of the building is depicted in Fig. 10, which also provides details such as the height of each floor and the cross-section of the columns and beams. For further specifics about this building, refer to the previous literature [40]. A total of 13 strong motion sensors were installed on the ground, second, third, and roof levels of this building. The recorded response data includes the behavior of the structure during three earthquakes: the 1987 Whittier Narrows earthquake, the 1991 Sierra Madre earthquake, and the 1994 Northridge earthquake.

The finite element model of the six-story building was constructed using OpenSees [37], as outlined in the previous literature [40]. The tributary seismic response masses were determined to be 235.6 tons per level, and a damping ratio of 0.03 was applied to the building. The finite element model of the building exhibited a period of 1.43 s, which closely aligned with the target period specified in the literature [40].

To simulate the structural response under earthquake ground motions, popular ground motions for Los Angeles [42] were employed. These ground motions varied in terms of probabilities of exceedance and time intervals. In total, 40 earthquake ground motions with a consistent

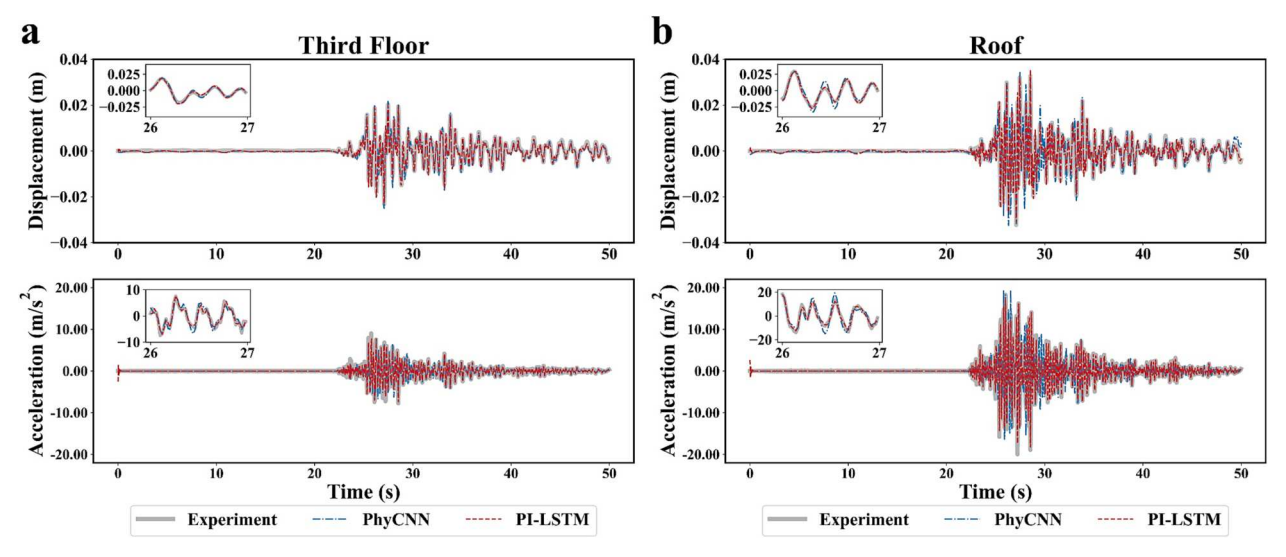


Fig. 9. Prediction performance of PhyCNN and PI-LSTM in terms of the (a) third floor and (b) roof.

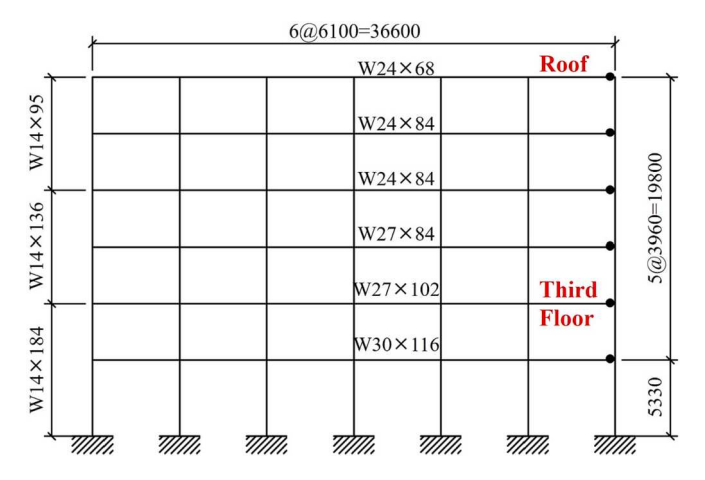


Fig. 10. Elevation of the six-story building (from [40]).

time interval of 0.02 s but different probabilities of exceedance were selected for the analysis. The ground motions comprised LA01-LA02, LA07-LA14, LA17-LA20 (10% probability of exceedance); LA21-LA22, LA27-LA30, LA37-LA40 (2% probability of exceedance); and LA45-LA60 (50% probability of exceedance). To obtain numerical simulation results for the six-story building, these earthquake ground motions were applied to the finite element model mentioned earlier. Fig. 11 illustrates one sample of the ground acceleration, structural displacement, structural velocity, and structural acceleration obtained from this

simulation. Out of the 40 samples, 20 samples were randomly selected from each group based on their corresponding proportion for use as training data. Additionally, 10 samples were allocated for validation purposes, and the remaining 10 samples were set aside as test data. For example, during the selection of training data, 7 samples were randomly chosen from the group consisting of the earthquake ground motion with a 10% probability of exceedance, 5 samples were selected from the group with a 2% probability of exceedance, and 8 samples were chosen from the group with a 50% probability of exceedance.

The primary objective of this numerical validation is to assess acceleration as the most commonly used indicator for structural health monitoring. The focus is on the third floor and roof of the depicted sixstory building (Fig. 10). Due to the complexity of directly calculating motion equation parameters, the PI-LSTM model illustrated in Fig. 4 could effectively model the structural response of various floors in the multi-story building. For comparison purposes, two models, PI-LSTM and LSTM, were utilized to simulate the structural response. Table 3 (Case 4) provides a summary of the information regarding PI-LSTM and LSTM. The inputs for both models were ground acceleration and the previous structural responses (displacement and mass-normalized restoring force), while the outputs were displacement and massnormalized restoring force. The predicted acceleration was derived from the second-order derivative of the predicted displacement. The data loss was determined by the variance between the predicted structural responses (acceleration and mass-normalized restoring force) and the results from numerical simulations, while the physics loss for PI-LSTM was based on adherence to physics constraints. Fig. 12 and Table 7 present the performance evaluation of PI-LSTM and LSTM in

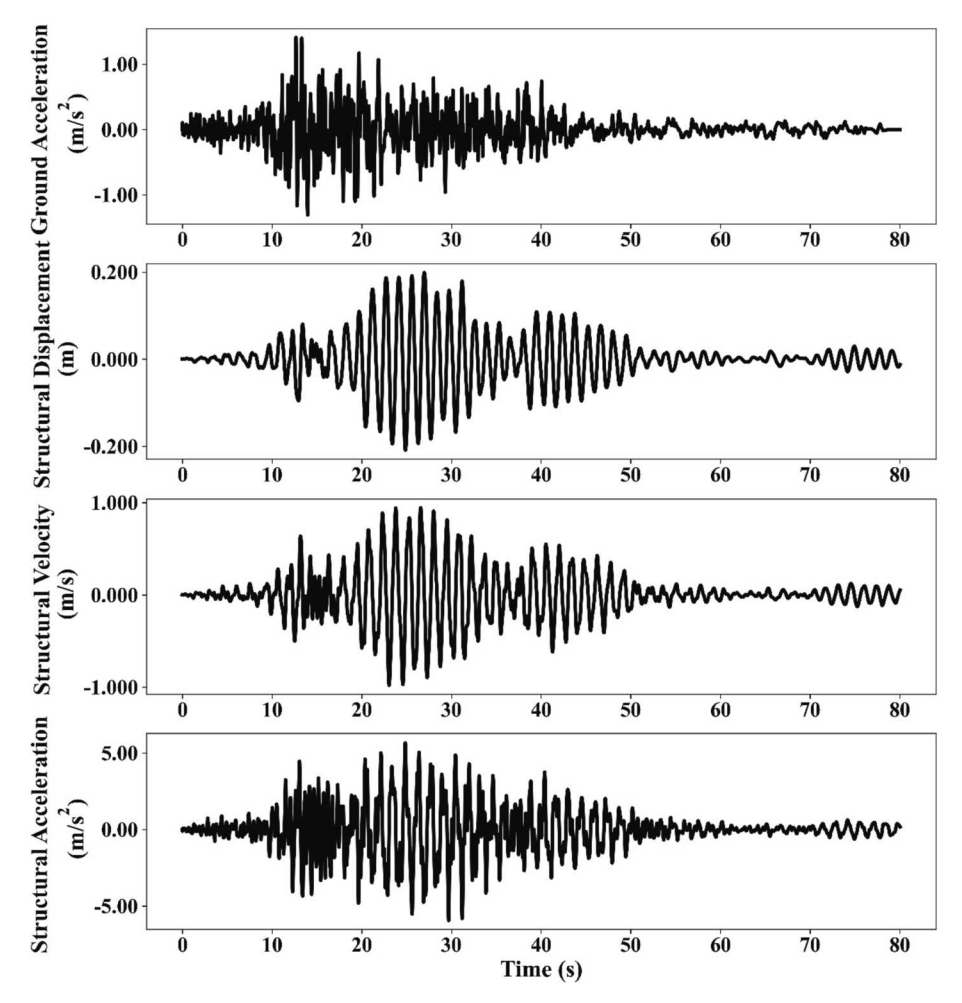


Fig. 11. Data for the ground acceleration, structural displacement, structural velocity, and structural acceleration.

predicting the structural responses for the third floor and roof, PI-LSTM outperformed LSTM significantly in terms of displacement accuracy, while its accuracy in acceleration prediction was only marginally higher than that of LSTM. Notably, PI-LSTM exhibited a narrower accuracy range for both displacement and acceleration compared to LSTM. Fig. 13 showcases the predictions of LSTM and PI-LSTM for the structural responses of the third floor and roof. PI-LSTM demonstrated superior performance in predicting acceleration compared to displacement. Although the predicted displacement amplitude of PI-LSTM was slightly lower than the numerical simulation results, it successfully captured the displacement trend with high accuracy. Consequently, PI-LSTM proves to be a precise and robust approach for modeling the structural response under ground motion.

5. Discussion

In this study, model comparisons and several case studies were conducted to assess the performance of the PI-LSTM network and validate its effectiveness. For the purpose of model comparison, PhyCNN, a successful physics-informed deep learning model introduced by Zhang et al. [8], was selected, as it exhibited strong performance and datasets, model codes, and results were readily available. Furthermore, Zhang et al. [30] also developed PhyLSTM, another impressive physicsinformed deep learning model for structural metamodeling of nonlinear structures. Several distinctions can be observed between PI-LSTM and PhyCNN/PhyLSTM, contributing to variations in the performance and computational efficiency:

- 1) Incorporation of physics knowledge: While all three models treat the equation of motion as a physics constraint, they differ in their considerations of the equation's form. First, for linear analysis, PI-LSTM's physics constraint involves stiffness and damping separately, while velocity and acceleration are calculated from the predicted displacement (Cases 2 and 3). In contrast, PhyCNN combines stiffness and damping into a single variable known as restoring force. Second, in nonlinear analysis, PI-LSTM's physics constraint comprises ground acceleration, predicted restoring force, and acceleration derived from the predicted displacement. PhyCNN, on the other hand, does not consider the equation of motion as a physics constraint. PhyLSTM incorporates three items similar to PI-LSTM, but it obtains acceleration and restoring force from different steps.
- 2) Input features: PI-LSTM utilizes two types of input features, namely ground acceleration and previous structural responses, which can be adjusted based on specific requirements (e.g., both displacement and acceleration, or only displacement, or only acceleration, or both

Table 7 Summary of the performance of LSTM and PI-LSTM.

Third Floor						
Metric	LSTM		PI-LSTM			
	Displacement	Acceleration	Displacement	Acceleration		
R^2	0.608 ± 0.028	0.911 ± 0.069	$\textbf{0.778} \pm \textbf{0.009}$	0.927 ± 0.037		
RMSE	0.024 ± 0.016	0.480 ± 0.308	0.018 ± 0.011	0.429 ± 0.206		
MAE	0.012 ± 0.007	0.239 ± 0.135	0.009 ± 0.005	0.210 ± 0.098		

1001				
Metric	LSTM		PI-LSTM	
	Displacement	Acceleration	Displacement	Acceleration
R^2	0.677 ± 0.053	0.833 ± 0.079	0.813 ± 0.011	0.865 ± 0.028
RMSE	0.054 ± 0.039	1.059 ± 0.765	0.040 ± 0.027	0.919 ± 0.530
MAE	0.026 ± 0.016	0.512 ± 0.317	0.020 ± 0.012	$\textbf{0.449} \pm \textbf{0.232}$

Note: RMSE is the root mean squared error and MAE is the mean absolute error. The results shown in this table are the mean value \pm the standard deviation.

- displacement and restoring force). Conversely, both PhyCNN and PhyLSTM rely on a single input feature, namely ground acceleration.
- 3) Loss function (including physics loss) for nonlinear structural analysis: PI-LSTM's outputs for nonlinear structural analysis are restoring force and displacement, from which acceleration is computed based on the predicted displacement. The data loss encompasses the variance between predicted and measured acceleration and restoring force. The physics loss incorporates equations and includes ground acceleration, predicted restoring force, and acceleration derived from predicted displacement. These two losses are combined to form the final loss function. In comparison, PhyCNN's loss function solely considers the variance between predicted and measured acceleration. PhyLSTM's loss function consists of three components: data loss (predicted and measured displacement and velocity), "equality" loss (predicted and computed velocity), and physics loss (ground acceleration, acceleration, and restoring force).
- Operation logic: PI-LSTM employs a single LSTM architecture to directly compute structural responses, while PhyLSTM utilizes two or three LSTM architectures to incrementally calculate structural responses. For instance, PI-LSTM uses one LSTM architecture to directly predict displacement and restoring force. However, one variant of PhyLSTM (PhyLSTM2) initially employs one LSTM architecture to predict structural responses (displacement, velocity, and hysteretic parameters), followed by another LSTM architecture to predict restoring force based on the previously predicted structural responses. Consequently, these two models (PI-LSTM and PhyLSTM) differ in their operation logic and computational efficiency.

0.8

Acceleration

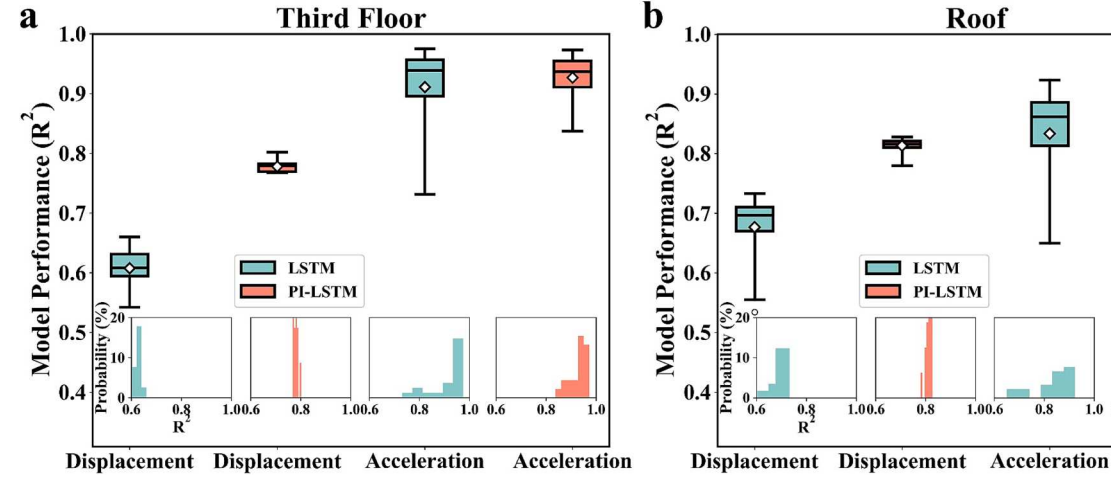


Fig. 12. Performance of LSTM and PI-LSTM for predicting the structural response in terms of the (a) third floor and (b) roof.

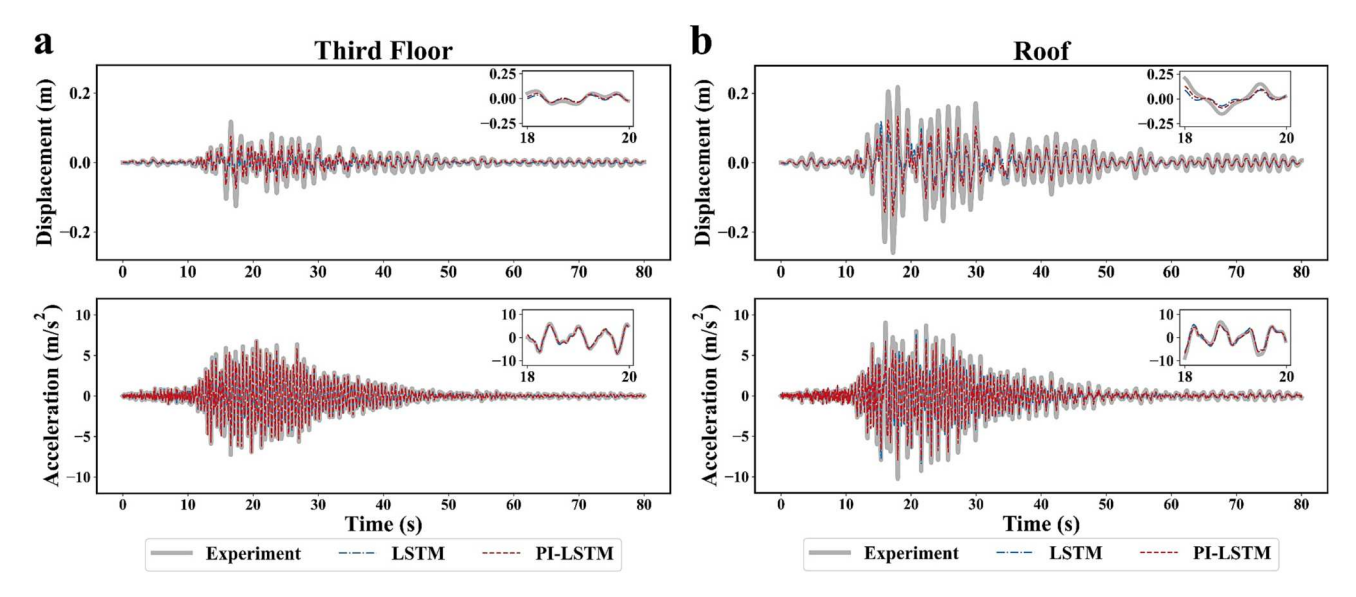


Fig. 13. Prediction performance of LSTM and PI-LSTM in terms of the (a) third floor and (b) roof.

 Core model architecture: PI-LSTM and PhyLSTM utilize LSTM architectures, whereas PhyCNN employs a CNN architecture.

The case studies conducted in this work encompassed both linear and nonlinear structural analyses, revealing distinct performance characteristics for the PI-LSTM network. Three linear SDOF case studies were specifically employed to assess the model's capabilities. In Case 1 (Section 3.2.1), the objective was to predict both displacement and acceleration, with both being considered as structural responses in the inputs and outputs (Table 3). Case 2 (Section 3.2.2) focused solely on predicting displacement, utilizing it as the only structural response in the inputs and outputs (Table 3). Case 3 aimed to predict acceleration exclusively. Unlike Cases 1 and 2, Case 3 employed displacement as the sole structural response in the inputs and outputs (Table 3), but the loss calculation was based on the acceleration derived from the predicted displacement. Table 4 presents the performances of LSTM and PI-LSTM in these three case studies, revealing notable distinctions. Firstly, PI-LSTM consistently outperformed LSTM across all case studies. Secondly, the accuracy of both LSTM and PI-LSTM was lower in Case 1 compared to Cases 2 and 3, which can be attributed to the different ranges of displacement and acceleration. Balancing two distinct output features poses challenges for the models, making them more prone to reaching local minima instead of global minima. Thirdly, LSTM exhibited similar accuracy in predicting displacement for both Case 2 and Case 3. However, its accuracy in predicting acceleration was higher in Case 3 compared to Case 2. This discrepancy arises due to the use of displacement as the input and output structural response in both cases, but the loss functions employed different structural responses. Case 2 utilized displacement, while Case 3 employed acceleration, leading LSTM to achieve higher accuracy in predicting acceleration in Case 3. Lastly, PI-LSTM demonstrated remarkably similar accuracy in predicting both displacement and acceleration in both Case 2 and Case 3 (R²: 0.953 and 0.958 for displacement, and 0.980 and 0.984 for acceleration). The accuracy of PI-LSTM in both displacement and acceleration surpassed that of LSTM in all cases, particularly for acceleration in Case 2. The inclusion of physics knowledge in the loss function, serving as a physics constraint, contributed to enhanced model performance, especially in terms of generalization for unknown structural responses (e.g., acceleration in Case 2). This highlights the advantage of physics-informed deep learning approaches.

In addition to linear structural analysis, the performance of the PI-LSTM network was examined through case studies involving nonlinear structural analysis. Both SDOF systems and multi-DOF systems, utilizing

experimental and numerical data, were considered. Compared to linear analysis, the PI-LSTM network adjusts the physics constraint (as depicted in Fig. 1 and Fig. 4) to accommodate the requirements of nonlinear analysis. For nonlinear analysis, PI-LSTM and LSTM exhibited differing performances. Firstly, PI-LSTM consistently outperformed LSTM across all case studies. Secondly, in comparison to linear analysis (Case 3), both PI-LSTM and LSTM achieved higher accuracy in predicting displacement for nonlinear analysis (Case 4). However, their accuracy in predicting acceleration declined after transitioning from linear to nonlinear analysis (Table 4), although PI-LSTM maintained higher accuracy than LSTM. This can be attributed to two factors: 1) The two outputs, namely displacement and restoring force, possess distinct ranges, making it challenging for the models to strike a balance between them and more prone to converging to local minima. 2) The incorporation of physics knowledge aids in improving the models' ability to generalize to unknown structural responses. Thirdly, multi-DOF nonlinear systems exhibit considerably greater complexity compared to SDOF linear or nonlinear systems. Consequently, both PI-LSTM and LSTM achieved lower accuracy in predicting displacement and acceleration for multi-DOF nonlinear systems (Table 4 and Table 7). Future investigations should encompass additional tests of physics-informed deep learning models on multi-DOF nonlinear systems to explore the applicability and generalization of these models.

6. Conclusion

Deep learning has emerged as a powerful and efficient tool for modeling structural responses. However, it often requires a large amount of training data, which can be time-consuming and challenging to collect. Additionally, purely data-driven models may not always satisfy the physics constraints of the problem at hand. To address these issues, this work introduces physics-informed deep learning, which incorporates scientific knowledge into deep learning models. In this study, a physics-informed long short-term memory (PI-LSTM) network was applied to structural response modeling. To validate the reliability of the PI-LSTM network, comparisons were made with existing physicsinformed deep learning models, namely PhyCNN and PhyLSTM, using numerical simulation results of SDOF systems and experimental results of the six-story building. The PI-LSTM network was also evaluated and validated using the regular LSTM model in four cases of the SDOF system and numerical simulation results for the six-story building. The results demonstrated that the PI-LSTM network exhibited higher accuracy and a narrower range of predictions compared to the PhyCNN model for both numerical simulation results of the SDOF system and experimental results of the six-story building. Furthermore, the PI-LSTM network outperformed the regular LSTM model in terms of accuracy and robustness for the SDOF system and the six-story building's numerical simulation results. These findings highlight the reliability and effectiveness of the PI-LSTM network for structural response modeling. In the future, this model can be further applied to model the structural response of various infrastructures, such as tunnels and bridges, under different loads or hazard events. By incorporating physics knowledge into deep learning, the PI-LSTM network holds promise for improving the accuracy and reliability of structural response predictions in various engineering applications.

Furthermore, it is important to note that this study primarily utilized data from a single building for training and evaluating the PI-LSTM network. Enhancing the generalization capabilities of the PI-LSTM network is a key area for future improvement. One possible approach is to incorporate additional building-specific information into the input data, which can help enhance the model's ability to generalize to different structures. Moreover, in this work, physics knowledge was integrated into the model through the physics constraint included in the loss function. However, there is potential to further investigate how physics knowledge can be effectively incorporated into the architecture of the proposed models. One potential avenue is to explore the concept of a physics layer, where the model explicitly incorporates physics principles as a distinct component within its architecture. Investigating the integration of physics knowledge at a deeper level can contribute to further improvements in the accuracy and robustness of models.

CRediT authorship contribution statement

Fangyu Liu: Conceptualization, Data curation, Formal analysis, Investigation, Methodology, Software, Validation, Visualization, Writing – original draft, Writing – review & editing. **Junlin Li:** Data curation, Formal analysis, Investigation, Methodology, Software, Validation, Writing – original draft, Writing – review & editing. **Linbing Wang:** Conceptualization, Funding acquisition, Investigation, Methodology, Project administration, Resources, Supervision, Writing – original draft, Writing – review & editing.

Declaration of Competing Interest

The authors declare that they have no known competing financial interests or personal relationships that could have appeared to influence the work reported in this paper.

Data availability

Data will be made available on request.

Acknowledgement

This work was supported by a grant from the National Science Foundation (No. 1939987). This work was also sponsored by a grant from the Center for Integrated Asset Management for Multimodal Transportation Infrastructure Systems (CIAMTIS), a US Department of Transportation University Transportation Center, under federal grant number 69A3551847103.

References

- [1] Li Y, Bao T, Gao Z, Shu X, Zhang K, Xie L, et al. A new dam structural response estimation paradigm powered by deep learning and transfer learning techniques. Struct Health Monit 2022;21(3):770–87.
- [2] Wu R-T, Jahanshahi MR. Data fusion approaches for structural health monitoring and system identification: past, present, and future. Struct Health Monit 2020;19 (2):552–86.

- [3] Guidorzi R, Diversi R, Vincenzi L, Mazzotti C, Simioli V. Structural monitoring of a tower by means of MEMS-based sensing and enhanced autoregressive models. Eur J Control 2014;20(1):4–13.
- [4] Dong Y, Li Y, Lai M. Structural damage detection using empirical-mode decomposition and vector autoregressive moving average model. Soil Dyn Earthq Eng 2010;30(3):133–45.
- [5] Gao Y, Mosalam KM, Chen Y, Wang W, Chen Y. Auto-Regressive Integrated Moving-Average Machine Learning for Damage Identification of Steel Frames. Appl Sci 2021;11:6084.
- [6] Lu X, McKenna F, Cheng Q, Xu Z, Zeng X, Mahin SA. An open-source framework for regional earthquake loss estimation using the city-scale nonlinear time history analysis. Earthq Spectra 2020;36(2):806–31.
- [7] Lu X, Cheng Q, Xu Z, Xu Y, Sun C. Real-time city-scale time-history analysis and its application in resilience-oriented earthquake emergency responses. Appl Sci 2019; 02:207.
- [8] Zhang R, Liu Y, Sun H. Physics-guided convolutional neural network (PhyCNN) for data-driven seismic response modeling. Eng Struct 2020;215:110704.
- [9] Zheng Z, Tian Y, Yang Z, Lu X. Hybrid framework for simulating building collapse and ruin scenarios using finite element method and physics engine. Appl Sci 2020; 10:4408
- [10] Wu W, Ge S, Yuan Y, Ding W, Anastasopoulos I. Seismic response of subway station in soft soil: Shaking table testing versus numerical analysis. Tunn Undergr Space Technol 2020:100:103389.
- [11] Yi Meng J, Lui EM. Seismic analysis and assessment of a skew highway bridge. Eng Struct 2000;22(11):1433–52.
- [12] Zhang R, Chen Z, Chen S, Zheng J, Büyüköztürk O, Sun H. Deep long short-term memory networks for nonlinear structural seismic response prediction. Comput Struct 2019;220:55–68.
- [13] Huang P, Chen Z. Deep learning for nonlinear seismic responses prediction of subway station. Eng Struct 2021;244:112735.
- [14] Li H, Wang T, Wu G. Dynamic response prediction of vehicle-bridge interaction system using feedforward neural network and deep long short-term memory network. Structures 2021;34:2415–31.
- [15] Liu F, Ding W, Qiao Y, Wang L. An artificial neural network model on tensile behavior of hybrid steel-PVA fiber reinforced concrete containing fly ash and slag power. Front Struct Civ Eng 2020;14(6):1299–315.
- [16] Liu F, Ye Z, Wang L. Deep transfer learning-based vehicle classification by asphalt pavement vibration. Constr Build Mater 2022;342:127997.
- [17] Liu J, Liu F, Zheng C, Zhou D, Wang L. Optimizing asphalt mix design through predicting the rut depth of asphalt pavement using machine learning. Constr Build Mater. 2022;356:129211.
- [18] Raissi M, Perdikaris P, Karniadakis GE. Physics-informed neural networks: A deep learning framework for solving forward and inverse problems involving nonlinear partial differential equations. J Comput Phys 2019;378:686–707.
- [19] von Rueden L, Mayer S, Beckh K, Georgiev B, Giesselbach S, Heese R et al. Informed Machine Learning—A Taxonomy and Survey of Integrating Knowledge into Learning Systems. arXiv preprint arXiv:190312394. 2019.
- [20] Diligenti M, Roychowdhury S, Gori M. Integrating prior knowledge into deep learning. 2017 16th IEEE international conference on machine learning and applications (ICMLA): IEEE; 2017. p. 920-3.
- [21] Daw A, Karpatne A, Watkins W, Read J, Kumar V. Physics-guided neural networks (pgnn): An application in lake temperature modeling. arXiv preprint arXiv: 171011431. 2017.
- [22] Battaglia P, Pascanu R, Lai M, Jimenez RD. Interaction networks for learning about objects, relations and physics. Adv Neural Inf Proces Syst 2016;29.
- [23] Marino K, Salakhutdinov R, Gupta A. The more you know: Using knowledge graphs for image classification. arXiv preprint arXiv:161204844. 2016.
- [24] Lee K-II, Ros G, Li J, Gaidon A. Spigan: Privileged adversarial learning from simulation. arXiv preprint arXiv:181003756. 2018.
- [25] Sutskever I, Vinyals O, Le QV. Sequence to sequence learning with neural networks. Adv Neural Inf Proces Syst 2014;27.
- [26] Vinyals O, Toshev A, Bengio S, Erhan D. Show and tell: A neural image caption generator. Proceedings of the IEEE conference on computer vision and pattern recognition 2015. p. 3156-64.
- [27] Liu F, Meamardoost S, Gunawan R, Komiyama T, Mewes C, Zhang Y, Wang L. Deep learning for neural decoding in motor cortex. Journal of Neural Engineering 2022; 19(5):056021.
- [28] Dai G, Ma C, Xu X. Short-term traffic flow prediction method for urban road sections based on space-time analysis and GRU. IEEE Access 2019;7:143025–35.
- [29] Chen Y, Peng G, Zhu Z, Li S. A novel deep learning method based on attention mechanism for bearing remaining useful life prediction. Appl Soft Comput 2020; 86:105919.
- [30] Zhang R, Liu Y, Sun H. Physics-informed multi-LSTM networks for metamodeling of nonlinear structures. Comput Methods Appl Mech Eng 2020;369:113226.
- [31] Filiatrault A, Christovasilis IP, Wanitkorkul A, van de Lindt JW. Experimental seismic response of a full-scale light-frame wood building. J Struct Eng 2010;136 (3):246–54.
- [32] Kijewski-Correa T, Kwon DK, Kareem A, Bentz A, Guo Y, Bobby S, et al. SmartSync: An integrated real-time structural health monitoring and structural identification system for tall buildings. J Struct Eng 2013;139(10):1675–87.
- [33] Chen Su, Tang B, Zhao K, Li X, Zhuang H. Seismic response of irregular underground structures under adverse soil conditions using shaking table tests. Tunn Undergr Space Technol 2020;95:103145.
- [34] Paszke A, Gross S, Massa F, Lerer A, Bradbury J, Chanan G, et al. Pytorch: An imperative style, high-performance deep learning library. Adv Neural Inf Proces Syst 2019;32.

- [35] Kingma DP, Ba J. Adam: A method for stochastic optimization. arXiv preprint arXiv:14126980. 2014.
- [36] Chiou B, Darragh R, Gregor N, Silva W. NGA project strong-motion database. Earthq Spectra 2008;24(1):23–44.
- [37] McKenna F. OpenSees: a framework for earthquake engineering simulation. Comput Sci Eng 2011;13(4):58–66.
- [38] Li J, Hao H, Fan K, Brownjohn J. Development and application of a relative displacement sensor for structural health monitoring of composite bridges. Struct Control Health Monit 2015;22(4):726–42.
- [39] Haddadi H, Shakal A, Stephens C, Savage W, Huang M, Leith W et al. Center for engineering strong-motion data (CESMD). 14th World Conference on Earthquake Engineering, Beijing, China2008.
- [40] Kunnath SK, Nghiem Q, El-Tawil S. Modeling and response prediction in performance-based seismic evaluation: case studies of instrumented steel momentframe buildings. Earthq Spectra 2004;20(3):883–915.
- [41] Uniform Building Code U. International conference of building officials. Uniform Building Code, Whittier, California. 1997.
- [42] Somerville PG. Development of ground motion time histories for phase 2 of the FEMA/SAC steel project: SAC Joint Venture; 1997.